Back to basics: Nanomodulating calcium silicate hydrate gels to mitigate CO2 footprint of concrete industry

Item Type	Article
Authors	Wang, X.;Ding, S.;Ashour, Ashraf;Ye, H.;Thakur, V.K.;Zhang, L.;Han, B.
Citation	Wang X, Ding S, Ashour A et al (2023) Back to basics: Nanomodulating calcium silicate hydrate gels to mitigate CO2 footprint of concrete industry. Journal of Cleaner Production. 434: 139921.
DOI	https://doi.org/10.1016/j.jclepro.2023.139921
Publisher	Elsevier
Rights	© 2023 Elsevier Ltd. All rights reserved. Reproduced in accordance with the publisher's self-archiving policy. This manuscript version is made available under the CC-BY-NC-ND 4.0 license.
Download date	2025-04-26 02:03:22
Link to Item	http://hdl.handle.net/10454/19717

Back to basics: Nanomodulating calcium silicate hydrate gels to mitigate CO_2 footprint of concrete industry

Xinyue Wang [1], Siqi Ding [2], Ashraf Ashour [3], Hailong Ye [4], Vijay Kumar Thakur [5,6], Liqing Zhang [7], Baoguo Han [1,*]

[1] *School of Civil Engineering, Dalian University of Technology, Dalian, 116024 China*
[2] *School of Civil and Environmental Engineering, Harbin Institute of Technology, Shenzhen, Shenzhen 518055, China*
[3] *Faculty of Engineering & Informatics, University of Bradford, Bradford, BD7 1DP, UK*
[4] *Department of Civil Engineering, The University of Hong Kong, Pokfulam, Hong Kong*
[5] *Biorefining and Advanced Materials Research Center, SRUC (Scotland's Rural College), Kings Buildings, Edinburgh, EH9 3JG, UK*
[6] *School of Engineering, University of Petroleum & Energy Studies (UPES), Dehradun 248007, Uttarakhand, India*
[7] *School of Civil Engineering and Architecture, East China Jiaotong University, Nanchang 330013, China*
* Corresponding author: hanbaoguo@dlut.edu.cn, hithanbaoguo@163.com

Abstract: To realize the sustainable development of concrete, it is vital to mitigate its consumption and environmental footprint (especially the CO_2 footprint) from prolonging the service life through upgrading mechanical and durable performances of concrete. Incorporating nanofillers can effectively tailor the microstructures and performances of concrete. The hydrated calcium silicate (C-S-H) gels account for half of the volume of hardened Portland cement pastes, and they are the fundamental source of the overall properties of concrete. However, the underlying mechanisms of nanofillers on C-S-H gels remains unclear. Herein, this paper underpinned the role of 5 types of representative nanofillers in tailoring the nanostructure of C-S-H gels in cement composites. The research results demonstrated that through the nano-core effect; nanofillers induce the formation of two new C-S-H gels in outer hydration products, namely nano-core-shell element doped low-density C-S-H (NEDLD C-S-H) and nano-core-shell element doped high-density C-S-H (NEDHD C-S-H). The indentation modulus/hardness of NEDLD and NEDHD C-S-H reaches 25.4/0.80 GPa and 46.7/2.72 GPa, respectively. Such superior performances of NEDLD and NEDHD C-S-H derive from the existence of nano-core-shell elements in C-S-H gels rather than the increase in C-S-H packing density. In a short-range, nanofillers form nano-core-shell elements by adsorbing silica tetrahedrons during the hydration process, improving the mechanical properties of C-S-H basic building blocks. In the long-range, the nano-core-shell elements modify the nano-scale performances of C-S-H gels in outer hydration products due to the increase of C-S-H gels' integrality.

Keywords: Nanomodulation; Hydrated calcium silicate (C-S-H); Concrete; CO_2 footprint

1 Introduction

Carbon emission reduction has become a critical survival problem that humans must face and solve. As the most used construction material, concrete is vital to the development of human society but produces a considerable amount of carbon emission [1]. Over 90% of the concrete carbon emissions come from using raw materials, mainly cement. In 2020, China produced 2.476 billion tons of cement and emitted about 1.48 billion tons of carbon dioxide. China's total carbon emission was 10 billion tons in 2020, and cement carbon emission accounts for about 15% of the total [2-5]. According to the composition of carbon emissions in concrete industry, the technical route of carbon emission reduction of concrete includes three aspects [6, 7]: one is to decrease the amount of cement in concrete to directly achieve carbon emission reduction, for example, the utilization of supplement cementitious materials and industrial wastes [8-10], as well as alternative cementitious materials with low carbon emissions [11]; the other is to prolong the concrete service life through upgrading its performance, for instance, the carbon emissions can be halved if the service life is doubled [4, 5].

The performance of concrete lie on the nanoscale organizational structure of hydration products that make up concrete, rather than on the material itself [12]. So it is conceivable to tailor concrete performance through regulating the nanoscale structures of hydration products of cement. This move modifies the concrete's mechanical properties and durability without the increase of cement content, in other words, decreases the demand of cement under the promise of required performance, demonstrating the enormous potential for achieving the carbon footprint reduction in the concrete industry.

Calcium-silicate-hydrate (C-S-H) gels account for over 50 vol.% of hardened Portland cement, and they are fundamental source of the overall properties of concrete. Former studies [13, 14] demonstrated that the mechanical behavior of C-S-H gels shows nanogranular nature, namely, the C-S-H gels present an accumulation of some C-S-H building blocks with a characteristic particle size of 5 nm, and the packing form and particle-to-particle contact dominate its mechanical responses. According to the C-S-H building blocks' packing densities, classic studies [13–15] classified C-S-H gels into low-density calcium-silicate-hydrate (LD C-S-H) with a packing density of 0.64 and high-density calcium-silicate-hydrate (HD C-S-H) with a packing density of 0.74. Generally, LD and HD C-S-H gels are associated with outer and inner hydration products of hardened cement paste in concrete, respectively [15]. Vandamme et al. [16] identified a new type of C-S-H gels with a packing density of 0.87 in low water-to-binder concrete, known as ultra-high-density calcium-silicate-hydrate (UHD C-S-H). These various sorts of C-S-H gels provide cohesive force in concrete, which is the origin of mechanical performance of concrete [17]. Hence, following the bottom-up theory, it is unsurprisingly conceived to modify the structures and properties of C-S-H gels at the nanoscale for improving the performance of concrete at the macroscale. However, many studies have confirmed that the nanogranular nature and nanomechanical behaviors possessed by C-S-H gels are the Portland cement concrete’s intrinsic characteristics, not dependent on types of cement, mix proportions, curing conditions, etc. [18, 19]. Moreover, traditional approaches for reinforcing concrete, such as adding macro or micro fillers, are also helpless to modify C-S-H gels’ structures or enhance their mechanical properties [20–22].

As a new technological revolution, nanoscience infiltrates and impetus for the development of new generation concrete. The breakthroughs in nanotechnology have been beneficial in essentially upgrading the concrete performance, offering practical approaches to tailor C-S-H gels structures from the nanoscale [23–27]. Such improvement may even break through the concrete intrinsic limitations in conventional concepts [28–32]. In general, C-S-H gels in nano-engineered concrete show the characteristics of increased polymerization degree [33], refined pore structures [34], as well as optimized chemical compositions [35] in comparative terms with C-S-H gels in traditional concrete. However, existing studies have only demonstrated the overall changes of C-S-H gels in nano-engineered concrete. Little attention is conducted to effect and modification mechanisms of C-S-H gels on the nanoscale mechanical properties and nanogranular nature of C-S-H gels. Understanding the effect of nanofillers on C-S-H gels is undeniably critical to comprehending the intricate phenomena in nano-engineered concrete and further controlling and designing the performances of concrete for mitigating CO_2 footprint.

Therefore, this study investigates how nanofillers affect the nanoscale performances and nanogranular nature of C-S-H gels in hydration products of cement paste in concrete. It then explores the mechanical performance improvement of concrete tailored by incorporating nanofillers from a bottom-up approach. For these purposes, cement paste samples without/with nanofillers were characterized using a nanoindentation technique together with SEM and EDS tests to allow a determination of nanoscale performances and microstructures of C-S-H gels. Moreover, micromechanical analysis and molecular dynamics (MD) together with discrete element method (DEM) simulations, were employed for revealing the modification mechanisms for nanofillers to the performances of C-S-H gels and the link between C-S-H gel properties and macroscale mechanical performances of nano-engineered concrete.

2 Experimental, theoretical, and numerical methods

2.1 Experimental programs

2.1.1 Mix proportions

In this study, P·O 42.5 R Portland cement, grade II fly ash, silica fume, water reducer with a water reduction capacity of 30%, and nanofillers were used as raw materials to fabricate cement paste samples. Existing studies have exhibit that various nanofillers, such as nano-silica [36], nano-titania [37], carbon nanotubes [38], graphene [39], and nano boron nitride [40] are effective in modifying cement-based materials performance; Their morphologies are shown in Fig. 1(a). Herein, this study employed these 5 representative nanofillers to analyze the effect of nanofillers on C-S-H gels. The properties of raw materials used are listed in Tables 1–3.

Table 1. Chemical composition of cement

Chemical composition	CaO	SiO_2	Al_2O_3	Fe_2O_3	MgO	SO_3	Na_2O
Mass fraction (%)	61.13	21.45	5.24	2.89	2.08	2.05	0.77

Table 2. Chemical composition of fly ash

Chemical composition	CaO	SiO_2	Al_2O_3	Fe_2O_3	MgO
Mass fraction (%)	2.27	53.36	29.09	3.87	0.81

Table 3. Properties of nanofillers

Types	Morphology	Purity (%)	Diameter (nm)	Length (μm)	Thickness (nm)	Specific surface area (m^2/g)	Surface treatment
Nano-silica	Powder	⩾99	20	-	-	⩾600	-
Nano-titania	Powder	⩾96	20	-	-	-	Silica-coated
Carbon nanotubes	Tube	-	20-30	10-30	-	70	Nickel-coated
Multi-layer graphene	Sheet	-	<2000	-	1-5	500	-
Nano boron nitride	Sheet	-	<1000		5–100	19	-

Table 4 exhibits the mix proportions of cement pastes in this study. They are determined by reference to previous studies [41] for achieving good mechanical performance and workability of cement pastes modified with different nanofillers.

Table 4. Mix proportions of cement pastes

Nanofiller	Code	Mix proportions (mass ratio)					
		Cement	Fly ash	Silica fume	Water	Superplasticizer	Nanofiller
-	Blank	1	0.25	0.313	0.375	0.015	-
Nano-silica	S	0.970	0.25	0.313	0.375	0.020	0.030
Nano-titania	T	0.980	0.25	0.313	0.375	0.015	0.020
Carbon nanotubes	C	0.997	0.25	0.313	0.375	0.015	0.003
Multi-layer graphene	G	0.995	0.25	0.313	0.375	0.015	0.005
Nano boron nitride	B	0.997	0.25	0.313	0.375	0.015	0.003

2.1.2 Sample preparation

Sample preparation aims to flatten the surface as possible for maximizing the validity of nanoindentation results. Therefore, after fabricating cement paste samples (the detailed procedure may be found in [41]), the samples were pretreated using the following steps [42]: 1) The cement paste samples were cut into prismatic pieces measuring 5 mm×10 mm×10 mm; 2) Cylindrical phenolic resin were filled with the cut samples after drying at 50 ℃ for 24 h; 3) The surfaces of samples were ground with sandpapers from coarse to fine; 4) The ground samples were successively polished with 0.5 μm and 0.04 μm polishing agents on a velvet cloth; 5) The samples were cleaned using an ultrasonic device for cleaning the surfaces; 6) The samples were dried at 50 ℃ for 24 h prior nanoindentation tests. It is noted that ethanol was selected as the washing medium and cooling agent to avoid changes in hydration products during sample pretreatment process.

2.1.3 Measurements

This study employed nanoindentation technology together with SEM and EDS tests to identify the nanomechanical properties and microstructures of C-S-H gels and provide references for further analyzing nanofillers' modification mechanisms on C-S-H gels. For these purposes, on the one hand, the indentation depth should satisfy the 1/10 rule of thumb and scale separability condition to ensure the nanoindentation results can reflect the intrinsic characteristics of the phases in concrete [43]. On the other hand, the loading program should be carefully selected to eliminate the discreteness derived from the C-S-H gels' time-dependent characteristics. Therefore, a trapezoidal loading program was selected in the nanoindentation test. The load increased linearly from the initial contact between Berkovich indenter and sample to 4 mN at a constant loading speed of 1 mN/s; then, the load of 4 mN sustained for 30 s; finally, the load decreased at a constant loading speed of 1 mN/s. The representative indentation load-depth curves for various phases in cement pastes are depicted in Fig. 1 (b). The nanoindentation results are considered valid because the curve shapes are consistent with that in previous studies [18, 44, 45]. The indentation modulus M and hardness H are obtained by combining the continuum scale model and load-depth curves through the following equations [46]:

$$M \stackrel{\text{def}}{=} \frac{\sqrt{\pi}}{2\beta}\frac{S}{\sqrt{A_{\mathrm{c}}}} \tag{1}$$

$$H \stackrel{\text{def}}{=} \frac{P_{\max}}{A_{\mathrm{c}}} \tag{2}$$

where S equaling $(\mathrm{d}P/\mathrm{d}h)_{h=h_{\max}}$ represents the contact stiffness, β equaling 1.034 is a correction coefficient for Berkovich indenter, and A_{c} represents the indenter-sample contact area under the peak load.

To obtain nanoscale mechanical behaviors of different nanoscale phases in cement pastes, statistical methods were employed for quantitative analysis of nanoindentation results. As a prerequisite for using statistical methods, each nanoindentation should be independent, which can be regarded as an event in statistical analysis. Hence, referring to previous studies [47, 48], a 10 × 10 grid nanoindentation test was conducted on a randomly selected region for every sample with a 10-μm spacing. The M and H of different types of C-S-H gels were analyzed by using the deconvolution method based on a probability density function (PDF), as given in Formula (3) [16].

$$Find\ (\mu_J, s_J, f_J) \text{ from } \min \frac{1}{m}\sum_{i=1}^{m}\left(P_i - P(x_i)\right)^2, \text{ s.t. } \sum_{J=1}^{n} f_J = 1 \tag{3}$$

where μ_J, s_J and f_J are the mean value, standard deviation, and volume fraction of phase J ($J = 1, 2, \dots, n$), respectively. P_i and $P(x_i)$ represent the frequency density of nanoindentation results and probability distribution function at x_i, respectively. Note that the nanomechanical property of each phase was considered to satisfy Gaussian distribution in this study, as expressed in Formula (4).

$$P(x_i) = \sum_{J=1}^{n} \frac{f_J}{\sqrt{2\pi s_J^2}} exp\left[-\frac{(x_i - \mu_J)^2}{2s_J^2}\right] \tag{4}$$

In addition, this study introduced some constraints for ensuring the accuracy and repeatability of statistical analysis [49]. First, the synchronous minimization of indentation modulus and hardness frequency distribution analysis was carried out. Second, the bin number *m* and the unknown phase number *n* satisfied *m*>5*n*–1. Third, the μ and s of adjacent phases should satisfy Formula 5 to ensure the validity of deconvolution.

$$\mu_j + s_J < \mu_{j+1} - s_{J+1} \tag{5}$$

After the nanoindentation test, SEM and EDS were performed for characterizing the microstructures at the nanoindentation point. Note that before SEM/EDS characterization, the sample surfaces were covered by a platinum film to ensure the sample's conductivity.

2.2 Theoretical analysis method

C-S-H gels present nanogranular nature, and their mechanical responses can be calculated by micromechanics. The *M* of C-S-H gels is given by Equations (6)–(8) [16].

$$M = m_s \times \Pi_M(v_s, \eta, \eta_0) \tag{6}$$

$$m_s = \frac{E_s}{1 - v_s^2} \tag{7}$$

$$\Pi_M(v_s = 0.2, \eta, \eta_0 = 0.5) = 2\eta - 1 \geq 0 \tag{8}$$

where m_s is the indentation modulus assuming the packing density $\eta = 1$ determined by the C-S-H basic building block's modulus E_s and Poisson's ratio v_s. The values of $E_s = 59$ GPa [50] and $v_s = 0.2$ [16] are assumed in the current study. Moreover, *M* of C-S-H gelsis influenced by the minimum packing density of solids capable of withstanding external forces η_0 ($= 0.5$ [12]) and packing density η of C-S-H building blocks. Meanwhile, the H can be expressed as Formulas (9) to (13) [12, 16, 51].

$$H_i = h_s \times \Pi_H(\alpha_s, \eta_i, \eta_0) \tag{9}$$

$$h_s = c_s \times A(1 + B\alpha_s + (C\alpha_s)^3 + (D\alpha_s)^{10}) \tag{10}$$

$$\Pi_H(\alpha_s, \eta_i, \eta_0 = 0.5) = \Pi_1(\eta_i, \eta_0) + \alpha_s \times (1 - \eta) \times \Pi_2(\alpha_s, \eta_i, \eta_0) \tag{11}$$

$$\Pi_1(\eta_i, \eta_0) = \frac{\sqrt{2(2\eta - 1)} - (2\eta - 1)}{\sqrt{2} - 1} \times (1 + a(1 - \eta) + b(1 - \eta)^2 + c(1 - \eta)^3) \tag{12}$$

$$\Pi_2(\alpha_s, \eta_i, \eta_0) = \frac{2\eta - 1}{2}(d + e(1 - \eta) + f(1 - \eta)\alpha_s + g\alpha_s^3) \tag{13}$$

where h_s is the hardness assuming the packing density $\eta = 1$ related to cohesion c_s and friction coefficient α_s between neighboring C-S-H basic building blocks. The cohesion c_s and friction coefficient α_s equal to 0.44 GPa and 0.181, respectively [16]. Moreover, the coefficients in Formula (11) to (13) are all constants when nanoindentation test uses Berkovich indenter. The coefficients *A*, *B*, *C*, *D*, *a*, *b*, *c*, *d*, *e*, *f*, and *g* equal to 4.7644, 2.5934, 2.1860, 1.6777, –5.3678, 12.1933, –10.3071, 6.7374, –39.5893, 34.3216, and –21.2053, respectively [12, 51]. By applying micromechanics, the C-S-H gels' nanogranular nature of in nano-engineered concrete can be revealed based on nanoindentation results.

2.3 Numerical simulation strategy

2.3.1 Molecular dynamics (MD) simulation

Under the action of nanofillers, the nanoscale microstructures and chemical composition of hydration products of cement paste may vary significantly. Unfortunately, because of the limitation of experimental technique, monitoring the hydration process is still challenging at the nanoscale. Therefore, MD method is recently employed to explore the effect of nanofillers on the hydration process of cement [52, 53]. Considering the complex composition of cement-based systems, C-S-H gels, the uppermost production in cement pastes were selected in this study as the research object. The MD model [54, 55] was established according to the following steps: 1) Construction: where a CaO-SiO_2-H_2O system was constructed by putting 125 $Si(OH)_4$, 125 $Ca(OH)_2$, and 375 H_2O molecules into a periodic cubic lattice, as depicted in Fig. 1 (c), the Ca/Si ratio is selected based on experimental results; 2) Relaxation: where the system was relaxed for 100 ps under a canonical ensemble of 300 K, and further for 500 ps under an isothermal-isobaric ensemble of 300 K and 0 Pa; 3) Reaction: where the system was subjected to the dynamic calculation by using a reaction force field ReaxFF for 1000 ps under a canonical ensemble of 2000 K; 4) Annealing: where the system was cooled to 300 K under the condition of a canonical ensemble to obtain the final structures, as depicted in Fig. 1 (d). Fig. 1 (d) demonstrates that some $Si(OH)_4$ molecules were polymerized to form a chain structure composed of a series of silica tetrahedrons. Moreover, the velocity Verlet algorithm was used throughout for solving equations of the above process. The detailed information about ensemble, reaction force field ReaxFF, and other related knowledge of molecular dynamics can refer to in the literature [56-58].

Additionally, because the size of nanofillers is much larger than that of the simulation area, the size of nanofillers in MD model was reduced to approximately 300 atoms, as shown in Fig. 1 (e). On the basis of the above MD model, the influence of nanofillers on cementitious composites' hydration products was discussed by analyzing the reaction evolution and product distribution.

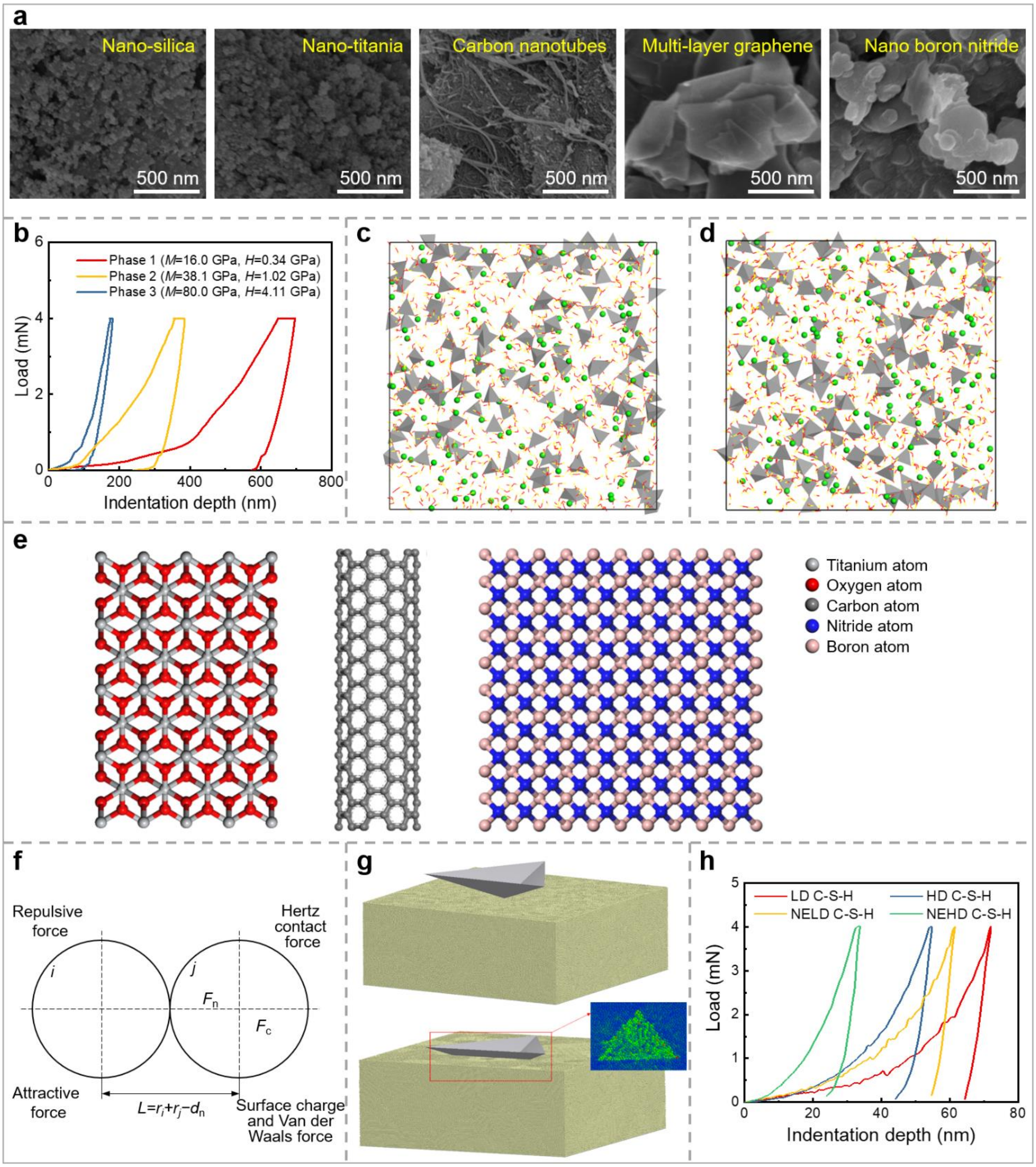

172

Fig. 1 Experimental, theoretical, and numerical methods and typical results. (a) Morphology of nanofillers; (b) Characteristic indentation load-depth curves of nanoidentation tests; (c) and (d) Configurations of CaO-SiO_2-H_2O system in initial and after-reaction MD model, respectively (in which gray tetrahedrons and green spheres represent silica tetrahedrons and Ca atoms, respectively); (e) Construction of nanofillers (namely nano-titania, carbon nanotube, graphene, nano boron nitride) in MD model; (f) Normal contact model between adjacent C-S-H basic building blocks in DEM model; (g) Schematic diagram of DEM model before Loading and Loaded to peak force; (h) Nanoindentation load-depth curve obtained from DEM simulation

173 *2.3.2 Discrete element method (DEM) simulation*

174 Micromechanics, assuming the C-S-H gels only consist of the C-S-H basic building blocks, can accurately analyze the

packing density of traditional C-S-H gels. Nonetheless, the micromechanics may be no longer valid after adding nanofillers, because new nanofiller particles/tubes/sheets appear in the system. Hence, DEM was employed to further investigate nanofillers' effect on the gels' nano-scale mechanical properties. Jennings [15] demonstrated that, C-S-H gels can be modelled as an accumulation of some spherical building blocks with a 5-nm characteristic particle size. In general, there are repulse forces caused by normal contact, friction forces caused by tangential sliding, charge force, and van der Waals force between adjacent C-S-H building blocks. The normal repulse force F_n can be described by the Hertz contact model [59], as expressed in Formula (14).

$$F_n = \frac{4}{3} E^* \sqrt{R^*} \delta_n^{3/2} \tag{14}$$

where E^* and R^* represent the equivalent Young's modulus and particle radius, respectively, as given in Formula (15) and (16) [60]; δ_n is the normal overlap.

$$\frac{1}{E^*} = \frac{(1 - v_i^2)}{E_i} + \frac{\left(1 - v_j^2\right)}{E_j} \tag{15}$$

$$\frac{1}{R^*} = \frac{1}{R_i} + \frac{1}{R_j} \tag{16}$$

where E_i/E_j, v_i/v_j, R_i/R_j respectively represent Young's modulus, Poisson's ratio, and radius of particle *i/j*. The values of Young's modulus, Passon's ratio, and radius of C-S-H spherical building blocks are taken as 70 GPa, 0.2, and 2.5 nm, respectively [61]. Moreover, the charge attraction force and van der Waals forces are the C-S-H gel strength's primary sources. The Johnson-Kendall-Roberts model [62] was used to describe the normal cohesion between particles, as given in Formula (17).

$$F_c = -4\sqrt{\pi \gamma E^*} a^{3/2} + \frac{4E^*}{3R^*} a^3 \tag{17}$$

where γ represents the surface energy, *a* is the interaction parameter that back-analyzed from Formula (18).

$$\delta_n = \frac{a^2}{R^*} - \sqrt{\frac{4\pi\gamma a}{E^*}} \tag{18}$$

Moreover, this study takes $r = 1.1d$ as the cut-off radius of normal cohesion and $F_{c,max} = 1.5$ nN as the maximum normal cohesive force to reduce computational cost [61]. Combined with Formulas (14) to (18), the normal contact model of C-S-H building blocks is established as depicted in Fig. 1 (f). The tangential friction force obeys Coulomb's law. The sliding friction coefficient μ_s and rolling friction coefficients μ_r between adjacent basic building globules in C-S-H gels equal to 0.65 and 5 [61], respectively.

Based on the above constitutive relationships, the DEM model of various sorts of C-S-H gels was established by the following steps: 1) Construction: where C-S-H building globules with a diameter of 5 nm were put into a box with a dimension of 800 nm × 800 nm × 300 nm, as shown in Fig. 1 (g), and the packing densities assigned 0.64 and 0.74 to LD and HD C-S-H [12]; 2) Property assignation: where the mechanical properties are assigned to C-S-H basic building globules; 3) Interaction assignation: where the interactions, such as cohesion and frication, are established between C-S-H basic building globules; 4) Loading: where the accumulation was loaded to 4 nm by a Berkovich indenter at a constant loading speed of 75 nm/s, as depicted in Fig. 1 (g), and unloaded at the same rate after holding 0.1 s; 5) Calculation: where the M and H of different types of C-S-H gels are calculated combined the indentation load-depth curves obtained from step 4 and Formulars (1) and (2). Fig. 1 (h) depicted the simulated load-indentation depth curves of various C-S-H gels.

By the above method, nano-titania, carbon nanotube, and nano boron nitride were included into the system to explore the effect of nanofillers on C-S-H gels' mechanical properties. Based on the nano-core theory [41, 49], nanofillers will be coated by C-S-H gels during hydration process. Therefore, this paper assumes that the surface of nanofillers is evenly covered with a 2.5 nm layer of C-S-H and forms nano-core-shell elements, and the contact between nano-core-shell elements and C-S-H building blocks is the same as that among C-S-H basic particles. In addition, because of the large size of carbon nanotubes and nano boron nitride, their length/area were reduced so that a single nanofiller can be placed in a 800 nm × 800 nm × 300 nm box at any angle.

3 Results and discussion

3.1 Nanomechanical characteristics of C-S-H gels

According to previous studies [18, 19], the nanoscale mechanical characteristics are the intrinsic characteristics of C-S-H gels, independent on types of cement, mix proportions, curing conditions, etc. Because the purpose of this work is to explore the effect of nanofillers on hydration products (especially C-S-H gels), the unhydrated binders were excluded from the deconvolution analysis. As demonstrated in the literature [18, 19], the phases were identified as unhydrated binder in cement pastes if their indentation modulus were higher than 50 GPa. The deconvolution results of M and H are illustrated in Fig. 2, Fig. 3, and Table 5.

The deconvolution results identified four phases existing in cement pastes without/with nanofillers. However, the C-S-H gels' types and contents, even the nanoscale mechanical properties, are quite different in nano-engineered cement pastes and plain cement paste.

1) Phase 1, with an indentation modulus $M = \mu_{M1} \pm s_{M1} =$ 8.1 ± 1.9 GPa and a hardness $H = \mu_{H1} \pm s_{H1} =$ 0.20 ± 0.15 GPa, identified as micro pore (MP) [18, 19, 22], occupied 9.3 vol.% of hydration products in plain cement paste. Moreover, no MP was observed in cement paste with nanofillers. Noteworthily, both M and H of MP itself are actually 0 GPa. The obtained M and H from deconvolution analysis reflect the nanomechanical properties of solid phases with

micropores. The MP is analyzed as an independent phase due to its reference value in multiscale numerical analysis [12].

2) Phase 2, with an indentation modulus $M = \mu_{M2} \pm s_{M2} =$ 19.7 ± 3.8 GPa and a hardness $H = \mu_{H2} \pm s_{H2} =$ 0.68 ± 0.08 GPa, identified as LD C-S-H [18, 19, 22], accounted for 8.0 vol.% of hydration products in plain cement paste. After adding nanofillers (except for nano-silica), the *M* and *H* of LD C-S-H, respectively, increases to 22.0–25.4 GPa and 0.74–0.90 GPa; the LD C-S-H content alters to 6.5–23.0 vol.%.

3) Phase 3, with an indentation modulus $M = \mu_{M3} \pm s_{M3} =$ 30.8 ± 3.0 GPa and a hardness $H = \mu_{H3} \pm s_{H3} =$ 1.05 ± 0.16 GPa, identified as HD C-S-H [18, 19, 22], occupied 61.0 vol.% of hydration products in plain cement paste. The addition of nanofillers showed no significant effect on the HD C-S-H's nanomechanical properties. Meanwhile, the incorporation of 3 wt.% nano-silica, 2 wt.% nano-titania, 0.3 wt.% carbon nanotubes, 0.5 wt.% multi-layer graphene, and 0.3 wt.% nano boron nitride decreases HD C-S-H content to 28.9%, 38.0%, 27.0%, 46.0%, and 37.5%, respectively.

4) Phase 4, with an indentation modulus $M = \mu_{M4} \pm s_{M4} =$ 37.5 ± 1.9 GPa and a hardness $H = \mu_{H4} \pm s_{H4} =$ 1.51 ± 0.16 GPa, identified as UHD C-S-H [18, 19, 22], accounted for 21.8 vol.% of hydration products in plain cement paste. After adding nanofillers, the nanomechanical properties of UHD showed no obvious changes, and the content increased to 28.4–43.1 vol.%. Note that UHD C-S-H possesses similar nanomechanical properties with calcium hydroxide (CH), indicating these two phases cannot be made a distinction through nanoindentation tests [16]. Considering the low water-binder ratio and large amounts of pozzolanic fillers in binder, it can be inferred that the CH content is low in samples [63, 64]. Hence, CH was ignored in deconvolution analysis.

5) Phase 5, with an indentation modulus *M* = 44.4–46.7 GPa and a hardness *H* = 1.70–2.72 GPa, occupied 5.7–24.7 vol.% of hydration products in cement paste with different types of nanofillers. This phase is considered as a new nano-induced hydration product for the following reasons. First, the nanomechanical properties of a given phase in cement-based composites are its intrinsic characteristics [18, 19], and the nanomechanical properties of the new phase differ from that of all raw materials and known hydration products in cement-based composites. Second, the new phase occupied 5.7–24.7 vol.% of hydration products in cement pastes with nanofillers, demonstrating the identified new phase is a major component of cement paste in nano-engineered concrete. Third, the new phase is only identified in samples with nanofillers.

To sum up, the nanofillers optimize the component of hydration products in cement pastes, as well as forms new hydration products. These phenomena may be attributed to the influences of nanofillers on the microstructures of LD and HD C-S-H through the nano-core effect [65], which is discussed in greater detail by using micromechanics analysis and MD/DEM simulations in sections 3.3 to 3.5.

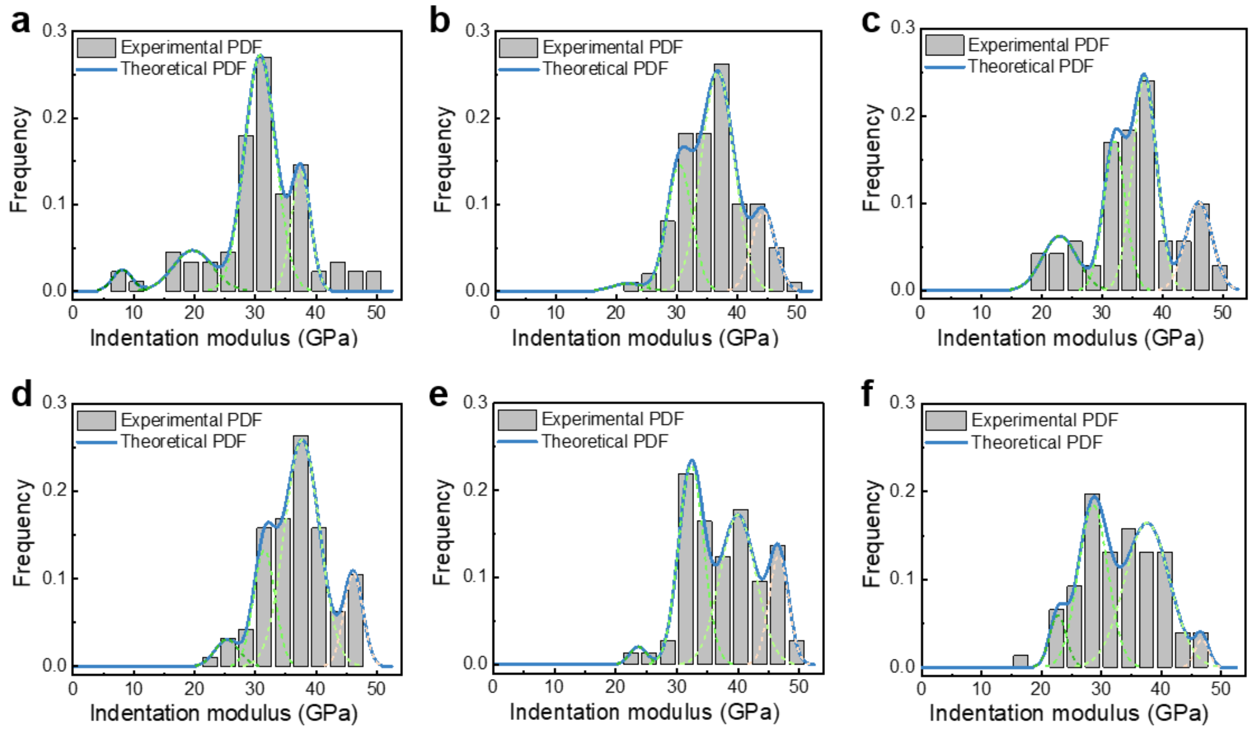

Fig. 2. Deconvolution results of the indentation modulus results. (a) Without nanofillers; (b) With nano-silica; (c) With nano-titania; (d) With carbon nanotubes; (e) With multi-layer graphene; (f) With nano boron nitride

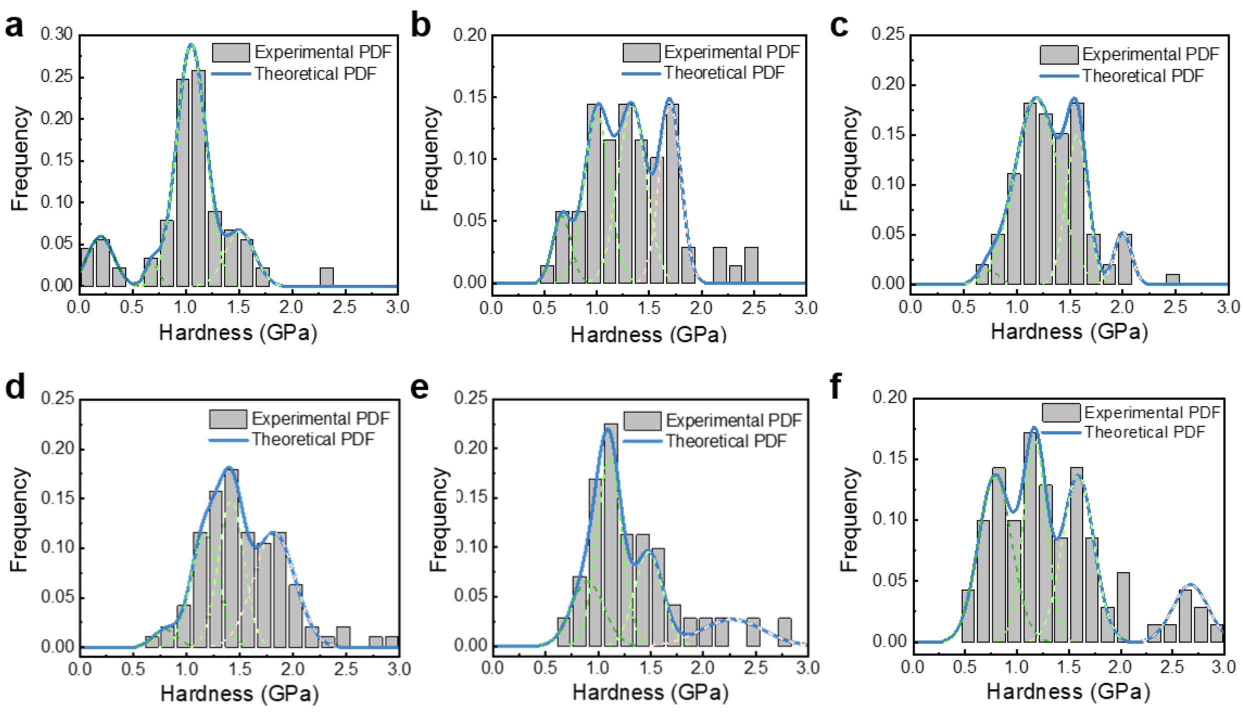

Fig. 3. Deconvolution results of the hardness results. (a) Without nanofillers; (b) With nano-silica; (c) With nano-titania; (d) With carbon nanotubes; (e) With multi-layer graphene; (f) With nano boron nitride

Table 4. Deconvolution results of *M* and *H*

Group	Phase 1			Phase 2			Phase 3			Phase 4			Phase 5		
	M (GPa)	*H* (GPa)	*f* (%)	*M* (GPa)	*H* (GPa)	*f* (%)	*M* (GPa)	*H* (GPa)	*f* (%)	*M* (GPa)	*H* (GPa)	*f* (%)	*M* (GPa)	*H* (GPa)	*f* (%)
Blank	8.1 ±	0.20 ±	9.3	19.7 ±	0.68 ±	8.0	30.8 ±	1.05 ±	61.0	37.5 ±	1.51 ±	21.8	–	–	–

	1.9	0.15		3.8	0.08		3.0	0.16		1.9	0.16				
S	–	–	–	22.0 ± 3.1	0.67 ± 0.10	6.5	30.5 ± 2.4	1.00 ± 0.14	28.9	36.8 ± 3.2	1.34 ± 0.16	40.2	44.4 ± 2.3	1.70 ± 0.12	24.3
T	–	–	–	23.0 ± 3.4	0.74 ± 0.11	7.1	32.1 ± 2.1	1.18 ± 0.24	38.0	37.0 ± 2.4	1.57 ± 0.12	39.7	46.0 ± 2.6	2.00 ± 0.10	15.2
C	–	–	–	25.4 ± 2.3	0.80 ± 0.13	5.2	31.5 ± 2.1	1.17 ± 0.15	27.0	37.7 ± 3.4	1.42 ± 0.14	43.1	46.2 ± 1.8	1.82 ± 0.23	24.7
M	–	–	–	23.7 ± 1.7	0.90 ± 0.18	10.6	32.3 ± 2.4	1.11 ± 0.14	46.0	40.0 ± 3.4	1.48 ± 0.16	28.4	46.6 ± 1.9	2.27 ± 0.35	15.0
B	–	–	–	22.7 ± 1.6	0.78 ± 0.18	23.0	28.6 ± 2.9	1.18 ± 0.14	37.5	37.6 ± 4.4	1.59 ± 0.18	33.9	46.7 ± 1.3	2.72 ± 0.27	5.7

3.2 Morphology and chemical composition of C-S-H gels

Figs. 4 show the morphology and chemical composition at the indentation point. As depicted in Fig. 4 (a), several nanoscale cracks appear at the indentation point, and the Ca/Si ratio equals 0.97. After adding nanofillers, the defects reduce at the indentation point in Fig. 4 (b)–(e). Noteworthily, the nanofillers with unique morphology (namely carbon nanotubes, multi-layer graphene, and nano boron nitride) are observed at the indentation point, as shown in Fig. 4 (c)–(e). The protrusions with the same shape as the nanofillers confirmed the presence of nanofillers at the indentation point, which may lead to C-S-H gels' superior nanomechanical properties due the high modulus and hardness of nanofillers. Meanwhile, the nanofillers are covered by hydration products as their morphologies in Fig. 4 (c) are quite different from their original morphologies in Fig. 1 (a). For example, the diameter of carbon nanotubes in Fig. 4 (c) is obvious larger than that of carbon nanotubes in Fig. 1 (a), indicating the carbon nanotubes are covered by hydration products. EDS results indicated that the protrusions at the indentation point in Fig. 4 (e) contained nano boron nitride sheets because of their high content of element nitride. Moreover, some nanoscale substances, which the indenter cannot flatten, appear near the edge of nano boron nitride in the indentation point, meaning that the substances are a kind of hard crystal. Owing to their hexagonal plate shape, the substances may be nanoscale CH crystals rather than C-S-H gels formed by the accumulation of C-S-H basic building blocks. As for the Ca/Si ratio, the ratio ranges are 0.09-1.63 after adding nanofillers, showing no obvious regularity. SEM/EDS results demonstrate that the presence of nanofillers may enhance the nano-scale mechanical properties of hydration products. The mechanisms and influences of these phenomena are investigated and discussed in detail in section 3.5.

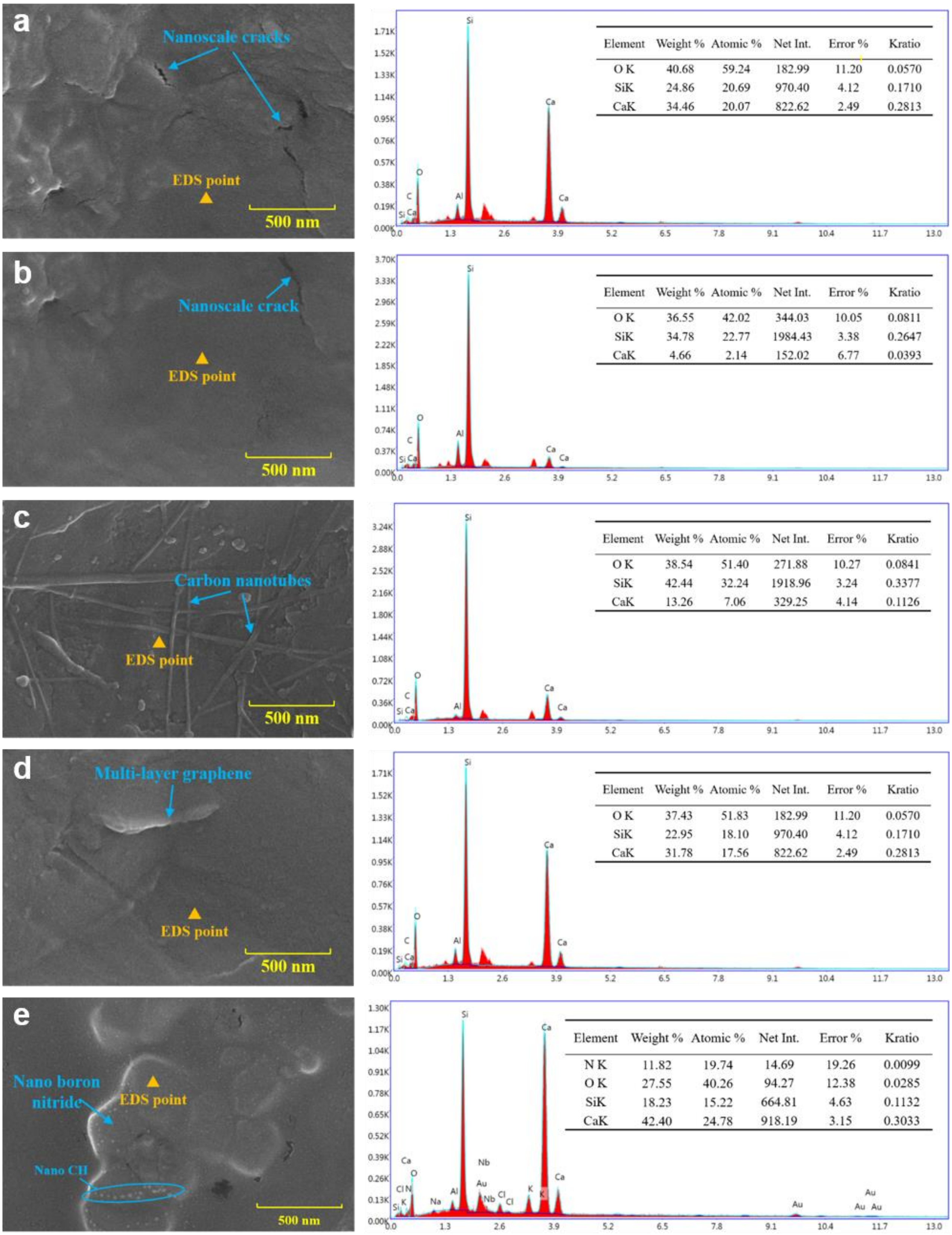

Fig. 4. Morphology and chemical composition at indentation point of sample without/with nanofillers. (a) Without nanofillers; (b) With nano-silica; (c) With carbon nanotube; (d) With multi-layer graphene; (e) With nano boron nitride

3.3 Packing density analysis

Combining nanoindentation deconvolution results with micromechanics, the packing densities of different C-S-H gels were obtained, as depicted in Fig. 5 and 6. The LD C-S-H's calculated packing density is 0.67, that approximates the random limit packing of spheress. The HD C-S-H's calculated packing density is 0.75, similar to the densest packing of spheres. As for UHD C-S-H, its packing density is 0.81, showing a packing characteristic of the two-scale random limit packing of 0.87. The packing densities of various C-S-H gels are consistent with those in former studies [16, 66], demonstrating that the nanogranular nature is the C-S-H gel inherent feature.

According to micromechanics, the nanofillers hardly affect the nanoscale mechanical properties of HD and UHD C-S-H. As demonstrated in former studies [12], the HD and UHD C-S-H mainly appear in inner hydration products that form in situ from binder particles. The nanofillers cannot enter the binder particles due to the steric hindrance effect [67]. Therefore, nanofillers cannot affect the mechanical properties of the HD and UHD C-S-H in inner products.

In contrast, LD C-S-H's M and H increase after adding nanofillers. Based on the micromechanics, the LD C-S-H's packing density in cement pastes containing nanofillers increases to 0.69–0.72. Moreover, a new phase with an indentation modulus of 44.4–46.7 GPa and a hardness of 1.70–2.72 GPa is identified in this study. The packing density of the new phase is 0.85–0.90, calculated according to micromechanics. These two phases occupy 22.3–30.8 vol.% in cement paste with nanofillers, which is close to the volume proportion of outer hydration products (28.1 vol.%, calculated from the water volume ratio to total volume during casting). These phenomena may be benefits to the improvement of outer hydration products owing to the availability of numerous nanofiller particles. According to the literature [68], nanofillers can adsorb hydration products owing to their high surface energy, forming nano-core-shell elements, i.e., nanofillers act as the nano cores, and the adsorbed hydration products serve as the shell. The nano-core-shell elements serve as a new type of C-S-H building blocks with superior mechanical properties, enhancing the nanomechanical behaviors of C-S-H gels in outer hydration products. Noteworthily, to distinguish the C-S-H gels in outer products in cement pastes with nanofillers from that without nanofillers, phases 2 and 5 (in Table 5) are identified as nano-core-shell element doped low-density (NEDLD) C-S-H and nano-core-shell element doped high-density (NEDHD) C-S-H, respectively.

After adding nanofillers into cement paste, the packing density of C-S-H gels obtained from indentation modulus is significantly different from that calculated from hardness. Because of the introduction of new nanofiller particles, the equations in mechanics cannot accurately describe the nanomechanical properties of C-S-H with nanofillers. The nanomechanical behaviors and granular nature of NEDLD and NEDHD C-S-H are therefore investigated by DEM simulation in section 3.5.

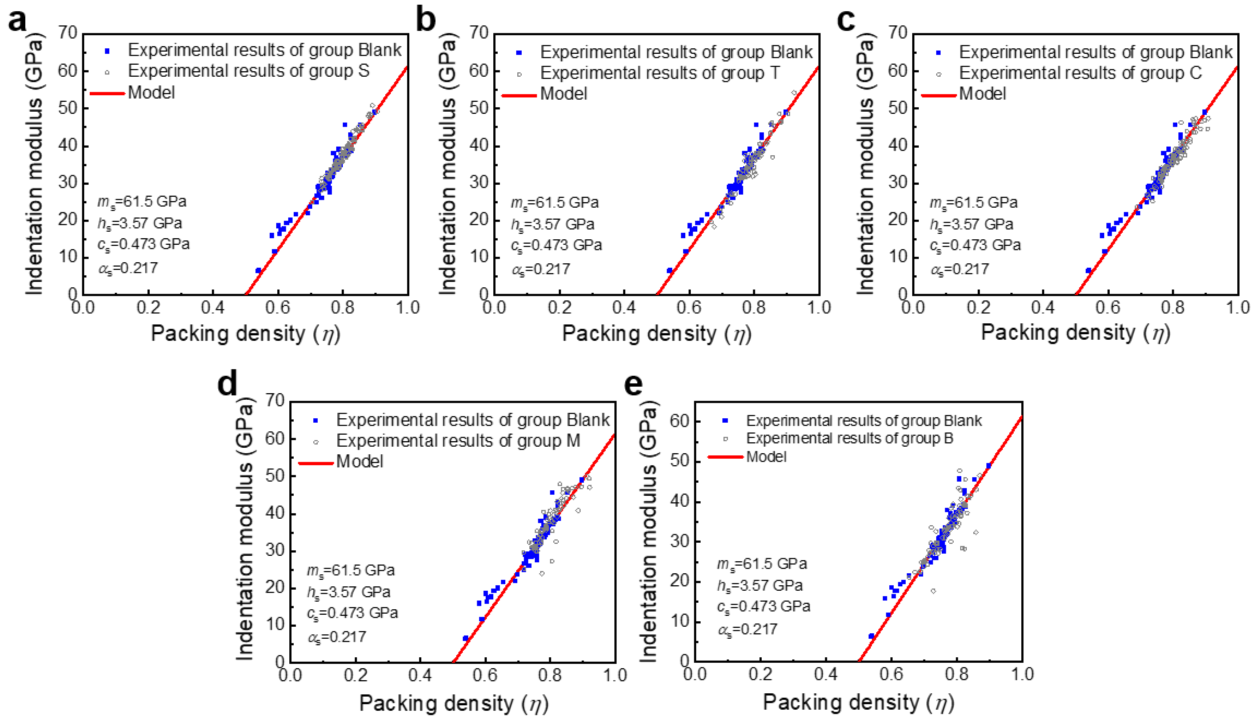

Fig. 5 Indentation modulus-packing density. (a) Without/with nano-silica; (b) Without/with nano-titania; (c) Without/with carbon nanotubes; (d) Without/with multi-layer graphene; (e) Without/with nano boron nitride

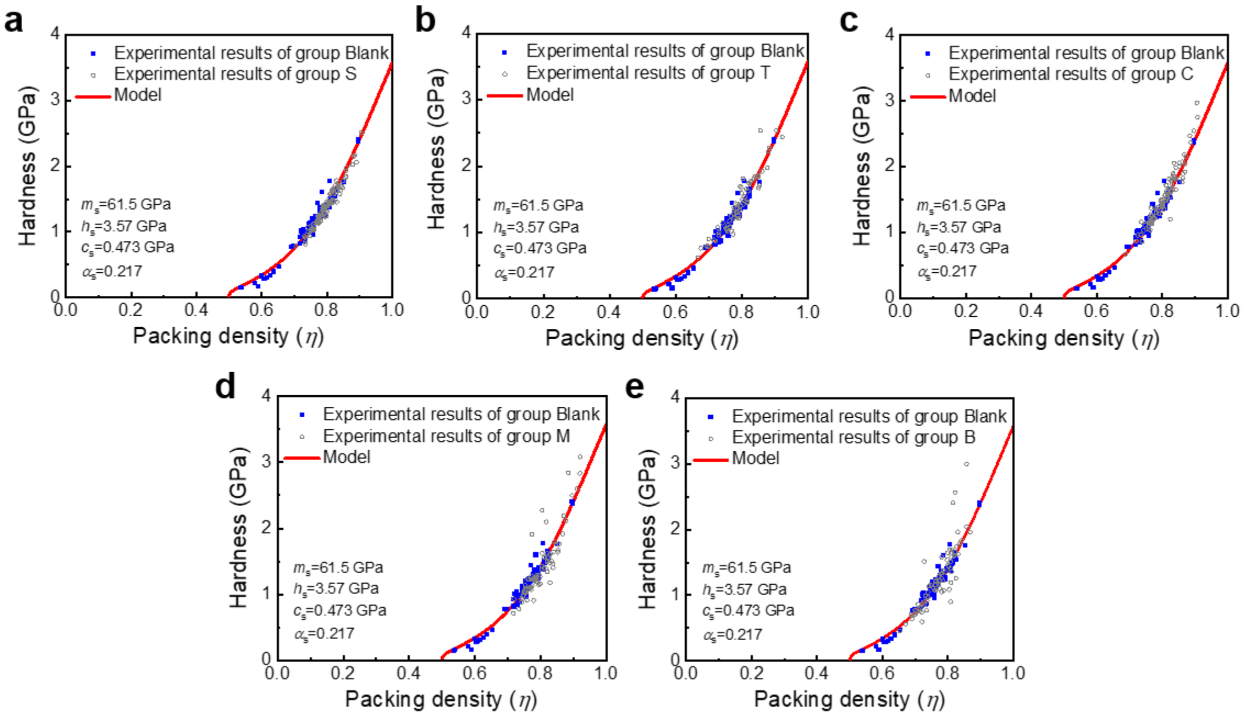

Fig. 6 Hardness-packing density. (a) Without/with nano-silica; (b) Without/with nano-titania; (c) Without/with carbon nanotubes; (d) Without/with multi-layer graphene; (e) Without/with nano boron nitride

3.4 Effect of nanofillers on C-S-H gels during hydration process

To reveal the effect of nanofillers on the hydration products, the structural evolution and product distribution were investigated based on the MD model.

1) Structural evolution

The formation of C-S-H gels is essentially the process of silica tetrahedron polymerization, i.e., forming Si-O-Si bond. Therefore, the structural evolution of the system can be inferred from the variation of Si-O-Si bond number with reaction time [69]. As demonstrated in Fig. 7 (a), the presence of carbon nanotube, multi-layer graphene, nano boron nitride has no noticeable effect on the formation of Si-O-Si bond number, indicating these nanofillers hardly affect forming C-S-H gels. Differently, adding nano-titania reduces the number of Si-O-Si bond. According to the model, the Ti atoms at the nano-titania surface can polymerize with silica tetrahedron and form Ti-O-Si bond, thus reducing the number of Si-O-Si bond.

2) Product distribution

The product distribution can be quantitatively analyzed and qualitatively observed by radial distribution function (RDF) and product distribution image, respectively. The RDF reflects the density of particles on the sphere with given particles as the center and *r* as the radius, as shown in Formula (19) [58].

$$g(r) = \frac{n(r)}{\rho_0 V} \approx \frac{n(r)}{4\pi r \rho_0 \delta_r} \tag{19}$$

where $n(r)$ is the number of particles in the spherical shell, ρ_0 is the ideal crystal density, δ_r is the thickness of the spherical shell. The RDF distributions of oxygen element in the CaO-SiO_2-H_2O post-reaction systems without/with nanofillers are shown in Fig. 7 (b). Fig. 7 (b) depicted that the RDF curve of oxygen element the CaO-SiO_2-H_2O post-reaction systems without nanofillers contains three peaks. The peaks appear near 0.97 Å, 1.64 Å, 2.05 Å, and 2.69 Å, corresponding to the H-O, Si-O, Ti-O and Ca-O bonds, respectively. Note that the interference function between RDF results and small-angle X-ray scattering test is the Fourier transform, which provides the link between experiment and MD model [58]. According to previous studies [70, 71], the position of peaks obtained from MD simulation is in a good agreement with that obtained from experiments, indicating that the MD simulation results in this study are valid. After adding nanofillers, the positions of the peaks may slightly shift, which is attributed to the interaction between particles changing the bond length between local atoms near nanofiller surface. However, the interaction does not change the type of the bond, that is, nanofiller hardly affects the process of hydration.

In addition to RDF analysis, the product distributions are also observed by images. The product distribution images display only the calcium, silicon, and nitrogen elements as well as nanofiller particles, but hide the oxygen and hydrogen elements, as depicted in Figs. 7 (c)-(g). The calcium and silicon elements in the system without nanofillers, as shown in Fig. 7 (c), are evenly distributed in lattice without obvious aggregation. In contrast, Figs. 7 (d)-(g) demonstrates that the presence of nanofillers can adsorb silica tetrahedrons and calcium ions, leading to the aggregation of calcium and silicon elements near the nanofillers. Moreover, the silica tetrahedrons tend to accumulate on the surface of nano boron nitride, while the calcium ions are easier to be adsorbed on the edge of nano boron nitride. These phenomena are consistent with the SEM results that indicate CH crystals tend to form and grow near the edge of nano boron nitride, as depicted in Fig. 4 (e). Such a phenomenon may derive from the van der Waals force and charge force. The charge on the edge of nano boron nitride is higher than that on the surface [72]. The particles near the edge of nano boron nitride are subjected to strong charge force, so the calcium ions with opposite charges are adsorbed on the edge. The calcium ions with opposite charge near the surface are subjected to a small charge force that is not strong enough to break through the steric hindrance effect. Hence, the surface of nano boron nitride mainly adsorbs silica tetrahedrons rather than calcium ions. In actual fresh cement pastes, the solubility and diffusion rates of calcium ions are much higher than silica tetrahedrons. The adsorbed calcium ions may be more than the simulation results at the early hydration process.

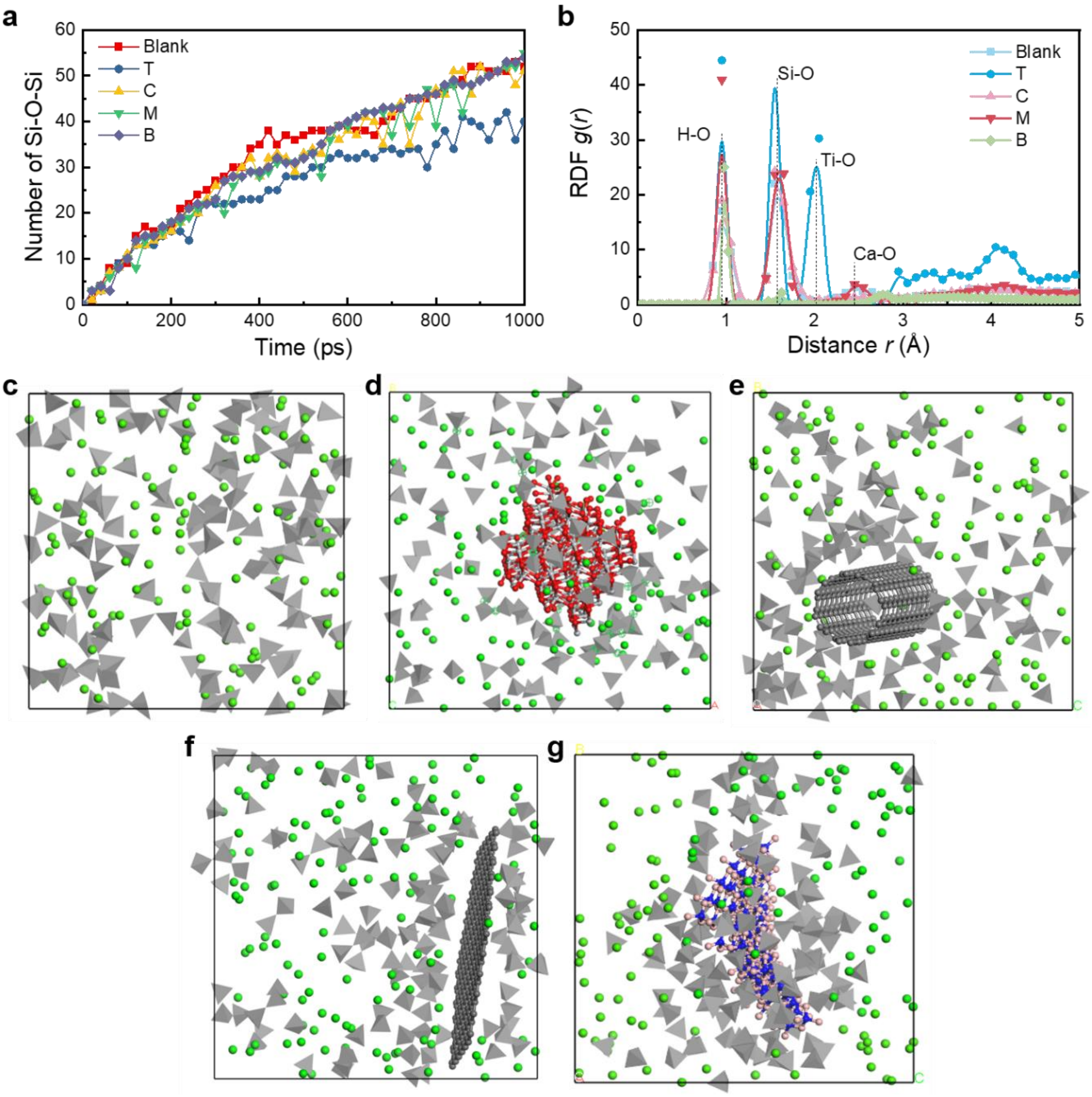

Fig. 7 Results of MD simulation. (a) Variation of Si-O-Si bond number vasus reaction time; (b) RDF distribution of oxygen element; Image of the post reaction system (c) without nanofillers, (d) With nano-titania, (e) With carbon nanotubes, (f) With multi-layer graphene and (g) With nano boron nitride

After early hydration of cement pastes, nanofillers together with the adsorbed calcium ions and silica tetrahedrons form numerous nano-core-shell elements, that is, nanofillers act as a nano core, and the adsorbed calcium ions and silica tetrahedrons form a shell. The nano-core-shell elements can be speculated to possess superior mechanical properties due to the existence of the nano core. The influences of these phenomena on the nanoscale mechanical properties of C-S-H gels are discussed in detail in the following sections.

3.5 Modification mechanisms of nanofillers on nanomechanical characteristics of C-S-H gels

Combining the load-indentation depth curves with Formulas (1) and (2), the calculated *M* and *H* were listed in Table 6, in which the *M* and *H* of LD and HD C-S-H derived from micromechanics analysis are in good agreement with experimental results, confirming the validity of established DEM model.

Unlike micromechanics analysis results, the DEM results demonstrate the packing densities of NEDLD and NEDHD C-S-H are slightly lower than those of LD and HD C-S-H. This finding indicates the improved the nanoscale mechanical properties of NEDLD and NEDHD C-S-H derives from the presence of nano-core-shell elements rather than the increase in C-S-H gels' packing density. The nano-core-shell elements replace some C-S-H building blocks, thus modifying the indentation modulus of C-S-H gels owing to their high modulus. Meanwhile, the nano-core-shell elements, together with the surrounding particles increase the C-S-H gels' integrality through the interaction between the particles, so as to increase the C-S-H gels' hardness.

Table 6. Comparison between simulation results and experimental/micromechanics results

Phase	Indentation modulus (GPa)		Hardness (GPa)		Packing density	
	Experimental results	DEM results	Experimental results	DEM results	Micromechanics analysis results	DEM results
LD C-S-H	19.7	21.3	0.68	0.69	0.67	0.64
LD C-S-H with nano-titania	23.0	24.4	0.74	0.80	0.69	0.64
LD C-S-H with carbon nanotubes	25.4	22.3	0.80	0.85	0.71	0.64
LD C-S-H with multi-layer graphene	23.7	18.8	0.90	0.60	0.71	0.64
LD C-S-H with nano boron nitride	22.7	29.2	0.78	0.81	0.70	0.64
HD C-S-H	30.8	29.1	1.05	1.07	0.75	0.74
HD C-S-H with nano-titania	44.4	34.9	2.00	2.18	0.86	0.74
HD C-S-H with carbon nanotubes	46.0	34.8	1.82	1.54	0.86	0.74
HD C-S-H with multi-layer graphene	46.2	36.6	2.27	2.78	0.88	0.74
HD C-S-H with nano boron nitride	46.7	52.6	2.72	3.18	0.90	0.74

According to the above results, Fig. 8 summarizes the underlying mechanisms of nanofillers on C-S-H gels. As demonstrated in Fig. 8, the nanofillers mainly affect the nanoscale mechanical characteristics of C-S-H gels in outer hydration products. The nanofiller particles, as demonstrated in MD simulation results, act as core sites to adsorb calcium ions and silica tetrahedrons, forming numerous nano-core-shell elements during the hydration process. Such formed elements help to reduce the calcium concentration in the early hydration solution, to reduce the nucleation of CH and further limit the growth of micron CH crystals. Meanwhile, the polymerization process of silica tetrahedron is not affected. Under this condition, most of the space of outer hydration products is occupied by nanofiller particles and surrounding adsorbed C-S-H building blocks, restricting the growth space of micron CH crystals in subsequent hydration process. Therefore, the nanofillers significantly refine the C-S-H gels and turns micron CH into nano CH in outer hydration products at the late stage of hydration.

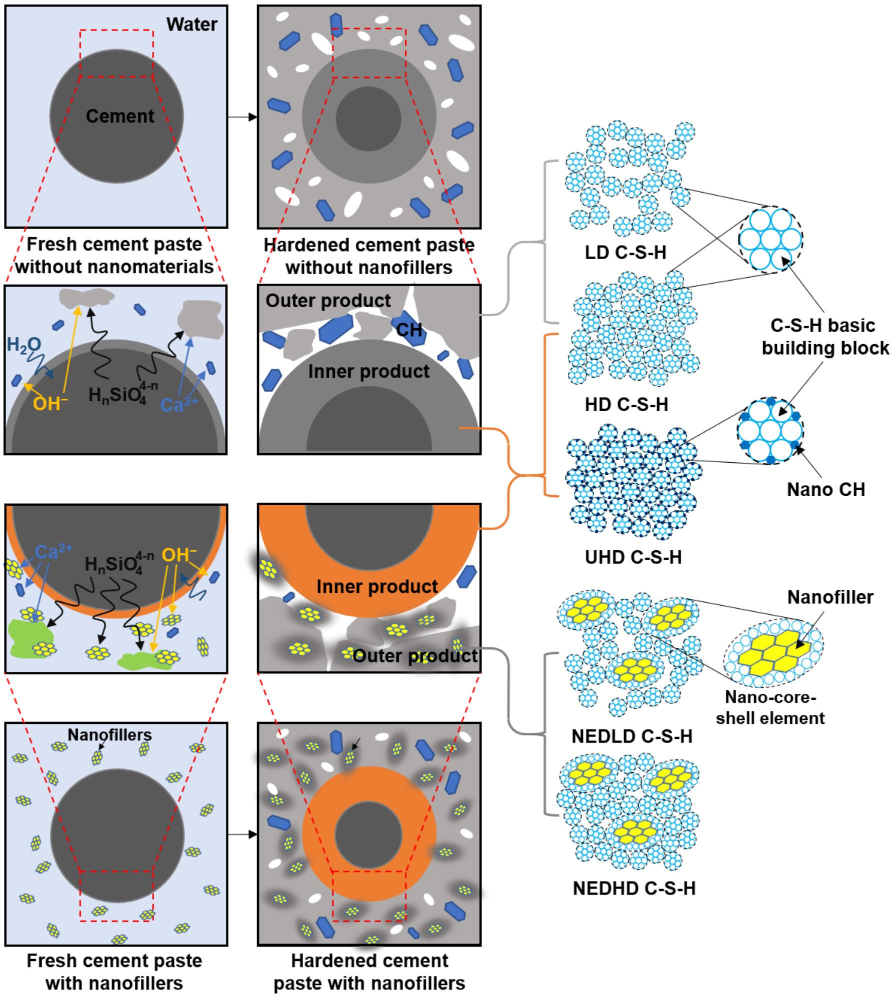

Fig. 8 The underlying mechanisms of nanofillers on C-S-H gels

Moreover, NEDLD and NEDHD C-S-H possess better nanoscale mechanical properties at lower packing densities than LD and HD C-S-H as demonstrated by micromechanics analysis and DEM simulation results. This finding can explain the role of nanofillers in improving the nanomechanical properties of C-S-H gels in outer hydration products. In the case of a constant mix proportion, the volume ratio of outer hydration products is basically unchanged before or after adding low content of nanofillers. Moreover, the presence of inactive nanofillers does not significantly change the hydration degree of cement pastes [40]. Therefore, the volume of outer hydration products and substances therein change little in cement pastes without or with nanofillers. Under these conditions, CH crystals formed by nanofillers adsorbed calcium ions, owing to their tiny size, can participate in the accumulation of C-S-H gels like the nanoscale CH crystals in UHD C-S-H [66], thus increasing the quantity of substances forming C-S-H gels in outer hydration products. Additionally, thanks to their low packing density and high-performance nature, NEDLD C-S-H and NEDHD C-S-H make more outer hydration product space occupied by C-S-H gels under the same amount of substances to decrease the defects and simultaneously improve the mechanical performance of outer hydration products.

A former study proposed the concept of the nano-core effect zone that considers the action zone of nanofillers composed of nanofillers themselves and adsorbed hydration products, i.e., the nano-core-shell elements [68]. Implementing this concept, the action zone in cement pastes accounts for about 0.44 vol.%, assuming that 0.4 vol.% nano boron nitride is added and the thickness of the shell is 2.5 nm. Such a small amount of action zone cannot explain the significant influence of the tiny content of nanofillers on the overall performances of cement pastes at the macroscale. Therefore, the former study only considered the short-range effect of nanofillers. The findings in the current study demonstrate that the nanofillers have a long-range effect on the cement pastes at the same time. On the one hand, nanofillers, combined with adsorbed hydration products, form nano-core-shell elements. Because of the existence of the hard core, the nano-core-shell elements modify the nanoscale mechanical properties of hydration products in a short-range. On the other hand, nanofillers can adsorb the ions in the early hydration solution, which refines and optimizes the hydration products near nanofiller particles. Moreover, the nano-core-shell elements and the surrounding particles increase the integrality of C-S-H gels through the interaction between the particles to increase the nanoscale mechanical properties of C-S-H gels under low packing densities.

The above findings have demonstrated nanofillers can modulate C-S-H gels, the major binding element in concrete, through modulating their nanogranular nature. Such modulation, on the one hand, enhances the network of C-S-H basic building blocks and the interaction among them, lessening the defects caused by internal volume changes (e.g. plastic, autogenous, drying, and carbonation shrinkages [73,74]) or external loads (e.g. compression, tension, and flexure loads [75–77]). On the other hand, the nanomodulation contributes to improve concrete durability due to the prevention of harmful media corrosion through refining larger pores into smaller ones in concrete at the nanoscale [34]. The aforementioned benefits lead to superior performance of nano-engineered concrete at the macroscale without increasing cement content [78–80], in other words, the ideal performance of concrete can be achieved with less cement through nanomodulation, thus cutting CO_2 emissions from reduced cement consumption or reducing CO_2 footprint by prolonging concrete service life.

4 Conclusions

This study provides evidence that nanofillers can improve intrinsic nanoscale mechanical performances of C-S-H gels of cement paste in concrete at the nanoscale. The nanofillers induce the formation of NEDLD and NEDHD C-S-H in outer hydration products. The indentation modulus/hardness of NEDLD and NEDHD C-S-H reached 25.4/0.80 GPa and 46.7/2.72 GPa, respectively. Meanwhile, the packing densities of NEDLD and NEDHD C-S-H are slightly lower than that of LD and HD C-S-H, respectively. The superior nanoscale mechanical performances of NEDLD and NEDHD C-S-H derive from the formation of nano-core-shell elements rather than the increase in the packing density. In a short-range, nanofillers together with adsorbed silica tetrahedrons form nano-core-shell elements during hydration of cement pastes in concrete, improving the mechanical properties of C-S-H basic building blocks. In the long-range, the nano-core-shell elements replace some C-S-H building blocks, thus improving the indentation modulus of C-S-H gels due to their high modulus. Moreover, the nano-core-shell elements, together with the surrounding C-S-H building blocks, increase the integrality of C-S-H gels through their interaction. The short-range and long-range effects proposed in this study provide a fundamental understanding of the superior nanoscale mechanical performances of C-S-H gels in concrete, guiding its design and applications. In addition to endowing C-S-H gels with superior mechanical properties at the nanoscale, the nanomodulation of C-S-H gels is conducive to upgrading the macroscale performance of concrete (e.g. strength, deformation behavior, volume stability, and harmful media resistance), on the basis of constant cement content. Consequently, a nano-engineered concrete, with superior mechanical properties, excellent durability and low cement need, can be developed through such nanomodulation, showing the great potential for mitigating the CO_2 footprint of concrete industry by reducing cement consumption and prolonging concrete service life.

Acknowledgements

The authors would like to thank the funding offered by the National Science Foundation of China (52308236, 51978127, 51908103, and 52368031), National Key Research and Development Program of China (2018YFC070560 and 2017YFC0703410), the China Postdoctoral Science Foundation (2022M720648, 2022M710973, 2022M713497).

References

[1] S. Ding, Y. Xiang, Y.Q. Ni, V.K. Thakur, X. Wang, B. Han, et al. In-situ synthesizing carbon nanotubes on cement to develop self-sensing cementitious composites for smart high-speed rail infrastructures, Nano Today 43 (2022) 101438. https://doi.org/10.1016/j.nantod.2022.101438.

[2] C.R. Gagg, Cement and concrete as an engineering material: An historic appraisal and case study analysis, Eng. Fail. Anal. 40 (2014) 114–140. https://doi.org/10.1016/j.engfailanal.2014.02.004.

[3] E. Elhacham, L. Ben-Uri, J. Grozovski, Y.M. Bar-On, R. Milo, Global human-made mass exceeds all living biomass,

Nature 588 (2020) 442–444. https://doi.org/10.1038/s41586-020-3010-5.

[4] F. Xi, S.J. Davis, P. Ciais, D. Crawford-Brown, D. Guan, C. Pade, et al. Substantial global carbon uptake by cement carbonation, Nat. Geosci. 9(12) (2016) 880–883. https://doi.org/10.1038/ngeo2840.

[5] A.E. Fenner, C.J. Kibert, J. Woo, S. Morque, M. Razkenari, H. Hakim, X. Lu, The carbon footprint of buildings: A review of methodologies and applications, Renewable Sustainable Energy Rev. 94 (2018) 1142–1152. https://doi.org/10.1016/j.rser.2018.07.012.

[6] R. Liu, H. Xiao, S. Guan, J. Zhang, D. Yao. Technology and method for applying biochar in building materials to evidently improve the carbon capture ability. J. Clean. Prod. 273 (2020) 123154. https://doi.org/10.1016/j.jclepro.2020.123154.

[7] D. Lu, X. Jiang, Z. Tan, B. Yin, Z. Leng, J. Zhong, Enhancing sustainability in pavement Engineering: A-state-of-the-art review of cement asphalt emulsion mixtures, Clean. Mater. (9) 2023 100204. https://doi.org/10.1016/j.clema.2023.100204.

[8] J. He, R. Xiao, Q. Nie, J. Zhong, B. Huang. High-volume coal gasification fly ash–cement systems: Experimental and thermodynamic investigation. Constr. Build. Mater. 377 (2023) 131082. https://doi.org/10.1016/j.conbuildmat.2023.131082.

[9] R. Xiao, B. Huang, H. Zhou, Y. Ma, X. Jiang. A state-of-the-art review of crushed urban waste glass used in OPC and AAMs (geopolymer): Progress and challenges. Clean. Mater. 4 (2022) 100083. https://doi.org/10.1016/j.clema.2022.100083.

[10] D. Lu, D. Wang, Y. Wang, J. Zhong, Nano-engineering the interfacial transition zone between recycled concrete aggregates and fresh paste with graphene oxide, Constr. Build. Mater. 384 (2023) 131244. https://doi.org/10.1016/j.conbuildmat.2023.131244.

[11] R. Xiao, X. Jiang, M. Zhang, P. Polaczyk, B. Huang. Analytical investigation of phase assemblages of alkali-activated materials in CaO-SiO_2-Al_2O_3 systems: The management of reaction products and designing of precursors. Mater. Design 194 (2020) 108975. https://doi.org/10.1016/j.matdes.2020.108975.

[12] G. Constantinides, F.J. Ulm, The nanogranular nature of C-S-H, J. Mech. Phys. Solids 55 (2007) 64–90. https://doi.org/10.1016/j.jmps.2006.06.003.

[13] H.M. Jennings, Colloid model of CSH and implications to the problem of creep and shrinkage, Mater. Struct. 37 (2004) 59–70. https://doi.org/10.1007/BF02481627.

[14] G. Constantinides, F.J. Ulm, The effect of two types of C-S-H on the elasticity of cement-based materials: Results from nanoindentation and micromechanical modeling, Cem. Concr. Res. 34 (2004) 67–80. https://doi.org/10.1016/S0008-8846(03)00230-8.

[15] H.M. Jennings, A model for the microstructure of calcium silicate hydrate in cement paste, Cem. Concr. Res. 30 (2000) 101–116. https://doi.org/10.1016/S0008-8846(99)00209-4.

[16] M. Vandamme, F.J. Ulm, P. Fonollosa, Nanogranular packing of C-S-H at substochiometric conditions, Cem. Concr. Res. 40 (2010) 14–26. https://doi.org/10.1016/j.cemconres.2009.09.017.

[17] W. Kurdowski. Cement and Concrete Chemistry, Springer, 2014. https://doi.org/10.1007/978-94-007-7945-7.

[18] S. Zhao, W. Sun, Nano-mechanical behavior of a green ultra-high performance concrete, Constr. Build. Mater. 63 (2014) 150–160. http://dx.doi.org/10.1016/j.conbuildmat.2014.04.029.

[19] C. Hu, Z. Li, A review on the mechanical properties of cement-based materials measured by nanoindentation, Constr. Build. Mater. 90 (2015) 80–90. http://dx.doi.org/10.1016/j.conbuildmat.2015.05.008.

[20] H. Lee, V. Vimonsatit, P. Chindaprasirt, Mechanical and micromechanical properties of alkali activated fly-ash cement based on nano-indentation, Constr. Build. Mater. 107 (2016) 95-102. http://dx.doi.org/10.1016/j.conbuildmat.2015.12.013.

[21] X. Wang, S. Jacobsen, J. He, Z. Zhang, S.F. Lee, H.L. Lein, Application of nanoindentation testing to study of the interfacial transition zone in steel fiber reinforced mortar, Cem. Concr. Res. 39 (2009) 701-715. https://doi.org/10.1016/j.cemconres.2009.05.002.

[22] C. Hu, Z. Li, Property investigation of individual phases in cementitious composites containing silica fume and fly ash, Cem. Concr. Compos. 57 (2015) 17-26. https://doi.org/10.1016/j.cemconcomp.2014.11.011.

[23] S. Sasmal, N. Ravivarman, B.S. Sindu, K. Vignesh, Electrical conductivity and piezo-resistive characteristics of CNT and CNF incorporated cementitious nanocomposites under static and dynamic loading, Compos. A-Appl. Sci. Manuf. 100 (2017) 227–243. https://doi.org/10.1016/j.compositesa.2017.05.018.

[24] D. Lu, Y. Huo, Z. Jiang, J. Zhong, Carbon nanotube polymer nanocomposites coated aggregate enabled highly conductive concrete for structural health monitoring, Carbon 206 (2023) 340-350. https://doi.org/10.1016/j.carbon.2023.02.043.

[25] D. Dimov, I. Amit, O. Gorrie, M.D. Barnes, N.J. Townsend, A.I.S. Neves, et al. Ultrahigh performance nanoengineered graphene-concrete composites for multifunctional applications, Adv. Funct. Mater. 28 (2018) 1705183. https://doi.org/10.1002/adfm.201705183.

[26] W. Meng, K.H. Khayat, Effect of graphite nanoplatelets and carbon nanofibers on rheology, hydration, shrinkage, mechanical properties, and microstructure of UHPC, Cem. Concr. Res. 105 (2018) 64–71. https://doi.org/10.1016/j.cemconres.2018.01.001.

[27] B. Han, L. Zhang, J. Ou. Smart and Multifunctional Concrete toward Sustainable Infrastructures, Springer, 2017. https://doi.org/10.1007/978-981-10-4349-9.

[28] B. Han, S. Ding, X Yu, Intrinsic self-sensing concrete and structures: A review, Measurement 59 (2015) 110–128. https://doi.org/10.1016/j.measurement.2014.09.048.

[29] D. Lu, D. Wang, J. Zhong, Highly conductive and sensitive piezoresistive cement mortar with graphene coated aggregates and carbon fiber, Cem. Concr. Compos. 134 (2022) 104731. https://doi.org/10.1016/j.cemconcomp.2022.104731.

[30] E. García-Macías, F. Ubertini, Earthquake-induced damage detection and localization in masonry structures using smart bricks and Kriging strain reconstruction: A numerical study: Earthquake-induced damage detection using smart-bricks, Earthq. Eng. Struct. Dyn. 48 (2019) 548–569. https://doi.org/10.1002/eqe.3148.

[31] D. Lu, Z. Leng, G. Lu, D. Wang, Y. Huo, A critical review of carbon materials engineered electrically conductive cement concrete and its potential applications, Int. J. Smart Nano Mater. 14 (2023) 189-215. https://doi.org/10.1080/19475411.2023.2199703.

[32] M. Krystek, A. Ciesielski, P. Samorì, Graphene-based cementitious composites: Toward next-generation construction technologies, Adv. Funct. Mater. 31 (2021) 2101887. https://doi.org/10.1002/adfm.202101887.

[33] J. Wang, B. Han, Z. Li, X. Yu, X. Dong, Effect investigation of nanofillers on C-S-H gel structure with Si NMR, J. Mater. Civil Eng. 31 (2019) 04018352. https://doi.org/10.1061/(ASCE)MT.1943-5533.0002559.

[34] J. Wang, S. Dong, C. Zhou, A. Ashour, B. Han, Investigating pore structure of nano-engineered concrete with low-field nuclear magnetic resonance, J. Mater. Sci. 56 (2021) 243–259. https://doi.org/10.1007/s10853-020-05268-0.

[35] A. Nazerigivi, A. Najigivi, Study on mechanical properties of ternary blended concrete containing two different sizes of nano-SiO_2, Compos. B-Eng. 167 (2019) 20–24. https://doi.org/10.1016/j.compositesb.2018.11.136.

[36] A. Khaloo, M.H. Mobini, P. Hosseini, Influence of different types of nano-SiO_2 particles on properties of high-performance concrete, Constr. Build. Mater. 113 (2016) 188-201. https://doi.org/10.1016/j.conbuildmat.2016.03.041.

[37] B. Han, Z. Li, L. Zhang, S. Zeng, X. Yu, B. Han, J. Ou, Reactive powder concrete reinforced with nano SiO_2-coated TiO_2, Constr. Build. Mater. 148 (2017) 104-112. https://doi.org/10.1016/j.conbuildmat.2017.05.065.

[38] S. Ding, X. Wang, L. Qiu, Y.Q. Ni, X. Dong, Y. Cui, et al. Self-sensing cementitious composites with hierarchical carbon fiber-carbon nanotube compositefillers for crack development monitoring of a maglev girder, small 19(9) (2022) 2206258. https://doi.org/10.1002/smll.202206258.

[39] H. Du, S. Pang. Enhancement of barrier properties of cement mortar with graphene nanoplatelet, Cem. Concr. Res. 76 (2015) 10-19. https://doi.org/10.1016/j.cemconres.2015.05.007.

[40] B. Han, S. Ding, J. Wang, J. Ou. Nano-Engineered Cementitious Composites: Principles and Practices, Springer, 2019. https://doi.org/10.1007/978-981-13-7078-6.

[41] X. Wang, Q. Zheng, S. Dong, A. Ashour, B. Han, Interfacial characteristics of nano-engineered concrete composites, Constr. Build. Mater. 259 (2020) 119803. https://doi.org/10.1016/j.conbuildmat.2020.119803.

[42] J. Xu, B. Wang, J. Zuo, Modification effects of nanosilica on the interfacial transition zone in concrete: A multiscale approach, Cem. Concr. Compos. 81 (2017) 1–10. https://doi.org/10.1016/j.cemconcomp.2017.04.003.

[43] Z. Luo, W. Li, K. Wang, S.P. Shah, Research progress in advanced nanomechanical characterization of cement-based materials, Cem. Concr. Compos. 94 (2018) 277–295. https://doi.org/10.1016/j.cemconcomp.2018.09.016.

[44] D. Davydov, M. Jirásek, L. Kopecký, Critical aspects of nano-indentation technique in application to hardened cement paste, Cem. Concr. Res. 41 (2011) 20–29. https://doi.org/10.1016/j.cemconres.2010.09.001.

[45] L. Xu, F. Deng, Y. Chi, Nano-mechanical behavior of the interfacial transition zone between steel-polypropylene fiber and cement paste, Constr. Build. Mater. 145 (2017) 619–638. https://doi.org/10.1016/j.conbuildmat.2017.04.035.

[46] W.C. Oliver, G.M. Pharr, An improved technique for determining hardness and elastic modulus using load and displacement sensing indentation experiments, J. Mater. Res. 7 (1992) 1564–1583. https://doi.org/10.1557/JMR.1992.1564.

[47] F.J. Ulm, M. Vandamme, H.M. Jennings, J. Vanzo, M. Bentivegna, K.J. Krakowiak, et al, Does microstructure matter for statistical nanoindentation techniques? Cem. Concr. Compos. 32 (2010) 92–99. https://doi.org/10.1016/j.cemconcomp.2009.08.007.

[48] M.J. DeJong, F.J. Ulm, The nanogranular behavior of C-S-H at elevated temperatures (up to 700 ℃). Cem. Concr. Res. 37 (2007) 1–12. https://doi.org/10.1016/j.cemconres.2006.09.006.

[49] X. Wang, S. Dong, Z. Li, B. Han, J. Ou, Nanomechanical characteristics of interfacial transition zone in nano-engineered concrete, Engineering 17 (2022) 99-109. https://doi.org/10.1016/j.eng.2020.08.025.

[50] S. Cariou, F.J. Ulm, L. Dormieux, Hardness-packing density scaling relations for cohesive-frictional porous materials, J. Mech. Phys. Solids 56 (2008) 924–952. https://doi.org/10.1016/j.jmps.2007.06.011.

[51] J. Sanahuja, L. Dormieux, G. Chanvillard, Modelling elasticity of a hydrating cement paste, Cem. Concr. Res. 37 (2007) 1427–1439. https://doi.org/10.1016/j.cemconres.2007.07.003.

[52] Y. Zhang, Q. Zhou, J.W. Ju, M. Bauchy. New insights into the mechanism governing the elasticity of calcium silicate hydrate gels exposed to high temperature: A molecular dynamics study. Cem. Concr. Res. 141 (2021) 106333. https://doi.org/10.1016/j.cemconres.2020.106333.

[53] Y. Zhang, S. Zhang, Q. Chen, Y. Shen, J.W. Ju, M. Bauchy. Insights into the effect of high temperature on the shear behavior of the calcium silicate hydrate by reactive molecular dynamics simulations. Int. J. Damage Mech. 31(7) (2022) 1096-1112. https://doi.org/10.1177/10567895221093395.

[54] A.S. Côté, A.N. Cormack, A. Tilocca, Influence of calcium on the initial stages of the sol-gel synthesis of bioactive glasses, J. Phys. Chem. B 120 (2016) 11773–11780. https://doi.org/10.1021/acs.jpcb.6b09881.

[55] C. Zhao, H. Liu, L. Guo, M. Bauchy, Precipitation of calcium-alumino-silicate-hydrate gels: The role of the internal stress, J. Chem. Phys. 153 (2020) 014501. https://doi.org/10.1063/5.0010476.

[56] T.P. Senftle, S. Hong, M.M. Islam, S.B. Kylasa, Y. Zheng, Y.K. Shin, et al, The ReaxFF reactive force-field: development, applications and future directions, NPJ Comput. Mater. 2 (2016) 15011. https://doi.org/10.1038/npjcompumats.2015.11.

[57] J. Xu, X. Chen, G. Yang, X. Niu, F. Chang, G. Lacidogna, Review of research on micromechanical properties of cement-based materials based on molecular dynamics simulation, Constr. Build. Mater. 312 (2021) 125389. https://doi.org/10.1016/j.conbuildmat.2021.125389.

[58] Y. Zhang, S. Zhang, X. Jiang, Q. Chen, Z. Jiang, J.W. Ju, et al. Insights into the thermal effect on the fracture toughness of calcium silicate hydrate grains: A reactive molecular dynamics study. Cem. Concr. Compos. 134 (2022) 104824. https://doi.org/10.1016/j.cemconcomp.2022.104824.

[59] H. Hertz, Ueber Die Berührung Fester Elastischer Krper, J. Reine Angew. Math. 92 (1882) 156–171. https://doi.org/10.1515/crll.1882.92.156.

[60] K.L. Johnson, Contact Mechanics, Cambridge University Press, Cambridge, 1985.

[61] P.C. Fonseca, H.M. Jennings, J.E. Andrade, A nanoscale numerical model of calcium silicate hydrate, Mech. Mater. 43 (2011) 408–419. https://doi.org/10.1016/j.mechmat.2011.05.004.

[62] K.L. Johnson, K. Kendall, A. Roberts, Surface energy and the contact of elastic solids, Prog. Theor. Phys. Supp. 324 (1971) 301–313. https://doi.org/10.2307/78058.

[63] D.P. Bentz, P.E. Stutzman, Evolution of porosity and calcium hydroxide in laboratory concretes containing silica fume, Cem. Concr. Res. 24 (1994) 1044–1050. https://doi.org/10.1016/0008-8846(94)90027-2.

[64] Y. Gao, C. Hu, Y. Zhang, Z. Li, J. Pan, Investigation on microstructure and microstructural elastic properties of mortar incorporating fly ash, Cem. Concr. Compos. 86 (2018) 315–321. https://doi.org/10.1016/j.cemconcomp.2017.09.008.

[65] X. Wang, S. Dong, A. Ashour, W. Zhang, B. Han, Effect and mechanisms of nanomaterials on interface between aggregates and cement mortars. Constr. Build. Mater. 240 (2020) 117942. https://doi.org/10.1016/j.conbuildmat.2019.117942.

[66] J.J. Chen, L. Sorelli, M. Vandamme, F.J. Ulm, G.C. Chanvillard, A coupled nanoindentation/SEM-EDS study on low water/cement ratio Portland cement paste: evidence for C-S-H/$Ca(OH)_2$ nanocomposites, J. Am. Ceram. Soc. 93 (2010) 1484–1493. https://doi.org/10.1111/j.1551-2916.2009.03599.x.

[67] O.A.M. Reales, P.A. Carisio, T.C.D. Santos, W. Pearl, R.D.T. Filho. Effect of pozzolanic micro and nanoparticles as secondary fillers in carbon nanotubes/cement composites, Constr. Build. Mater. 281 (2021) 122603. https://doi.org/10.1016/j.conbuildmat.2021.122603.

[68] B. Han, L. Zhang, S. Zeng, S. Dong, X. Yu, R. Yang, J. Ou, Nano-core effect in nano-engineered cementitious composites, Compos. A-Appl. Sci. Manuf. 95 (2017) 100–109. https://doi.org/10.1016/j.compositesa.2017.01.008.

[69] A. Tilocca, Structural models of bioactive glasses from molecular dynamics simulations, Proc. R. Soc. A. 465 (2009) 1003–1027. https://doi.org/10.1098/rspa.2008.0462.

[70] L.B. Skinner, S.R. Chae, C.J. Benmore, H.R. Wenk, P.J.M. Monteiro, Nanostructure of calcium silicate hydrates in cements, Phys. Rev. Lett. 104 (2010) 195502. https://doi.org/10.1103/PhysRevLett.104.195502.

[71] C. Meral, C.J. Benmore, P. Monteiro, The study of disorder and nanocrystallinity in C-S-H, supplementary cementitious materials and geopolymers using pair distribution function analysis, Cem. Concr. Res. 41 (2011) 696–710. https://doi.org/10.1016/j.cemconres.2011.03.027.

[72] Z. Balta, E.B. Simsek, Uncovering the systematical charge separation effect of boron nitride quantum dots on photocatalytic performance of $BiFeO_3$ perovskite towards degradation of tetracycline antibiotic, J. Environ. Chem. Eng. 9 (2021) 106567. https://doi.org/10.1016/j.jece.2021.106567.

[73] M. Segawa, A. Aili, I. Maruyama, Comparison of shrinkage and mass change of hardened cement paste under gradual drying and rapid drying, Cement 10 (2022) 100047. https://doi.org/10.1016/j.cement.2022.100047.

[74] H.M. Jennings, Colloid model of C-S-H and implications to the problem of creep and shrinkage, Mater. Struct. 37 (2004) 59-70. https://doi.org/10.1007/BF02481627.

[75] A. Goyal, I. Palaia, K. Ioannidou, F.J. Ulm, H.V. Damme, R.J.M. Pellenq, et al. The physics of cement cohesion, Sci. Adv. 7(32) (2021) 5882. https://doi.org/10.1126/sciadv.abg5882.

[76] A. Picker, L. Nicoleau, Z. Burghard, J. Bill, I. Zlotnikov, C. Labbez, et al. Mesocrystalline calcium silicate hydrate: A bioinspired route toward elastic concrete materials, Sci. Adv. 3(11) (2017) e1701216. https://doi.org/10.1126/sciadv.1701216.

[77] Z. Zhang, Y. Yan, Z. Qu, G. Geng, Endowing strength to calcium silicate hydrate (C-S-H) powder by high pressure mechanical compaction, Cem. Concr. Res. 159 (2022) 106858. https://doi.org/10.1016/j.cemconres.2022.106858.

[78] M. Şahmaran, F. Shaikh, G. Yıldırım, Recent Advances in Nano-Tailored Multi-Functional Cementitious Composites, Woodhead Publishing, 2022. https://doi.org/10.1016/C2020-0-01967-5.

[79] A. D'Alessandro, M. Tiecco, A. Meoni, F. Ubertini, Improved strain sensing properties of cement-based sensors through enhanced carbon nanotube dispersion, Cem. Concr. Compos. 115 (2020) 103842. https://doi.org/10.1016/j.cemconcomp.2020.103842.

[80] H. Du, S.D. Pang, Long-term influence of nanosilica on the microstructures, strength, and durability of high-volume fly ash mortar, 33 (2021) 04021185. https://doi.org/10.1061/(ASCE)MT.1943-5533.0003822.